

## Seismic refraction interferometry with a semblance analysis on the crosscorrelation gather

Dylan Mikesell<sup>1</sup> and Kasper van Wijk<sup>1</sup>

### ABSTRACT

Crosscorrelating wavefields recorded at two receivers to produce data as if one receiver was a source is commonly referred to as seismic interferometry, or the virtual source method. An artifact in seismic interferometry related to critically refracted waves allowed us to estimate the velocity in the refracting layer. In addition, we devised a new semblance analysis on the crosscorrelation of reflection and refraction energy to robustly estimate the depth and velocity of the slow layer, tested with a numerical example and field data from the Boise Hydrogeophysical Research Site.

### INTRODUCTION

The band-limited Green's function between two receivers is retrieved by crosscorrelating recorded wavefields from sources located on an enclosing surface around the two receivers. In exploration seismology, Green's function retrieval is called seismic interferometry (SI) of the crosscorrelation type (Wapenaar et al., 2004) or the virtual source method (Bakulin and Calvert, 2006). In the far-field approximation, the sum of the frequency-domain Green's function  $G$  and the complex conjugate  $G^*$  between two stations positioned at  $\mathbf{x}_{A,B}$  is

$$G(\mathbf{x}_A, \mathbf{x}_B) + G^*(\mathbf{x}_A, \mathbf{x}_B) \approx \oint_S \frac{2G^*(\mathbf{x}_A, \mathbf{s})G(\mathbf{x}_B, \mathbf{s})}{\rho(\mathbf{s})c(\mathbf{s})} dS, \quad (1)$$

where density and compressional wave velocity are  $\rho$  and  $c$ , respectively, and  $\mathbf{s}$  are monopole sources located on the closed surface  $S$ . We refer the reader to Wapenaar and Fokkema (2006) for a more complete description of this approximation.

With the survey geometry illustrated in Figure 1, we model the acoustic wavefield for 221 40-Hz Ricker wavelet sources at a 2.5 m

interval using the spectral element method (Komatitsch and Vilotte, 1998, Komatitsch and Tromp, 2002). We record the wavefield at 101 receivers spaced 4 m apart. The crosscorrelation gather is herein defined as the crosscorrelations between  $\mathbf{x}_A$  and  $\mathbf{x}_B$  for all sources. Summing the crosscorrelation gather for each receiver  $\mathbf{x}_A$ , we generate a virtual shot record (Mehta et al., 2008) as though there were a source at  $\mathbf{x}_B$ . Mikesell et al. (2009) use this model to show that when sources are not in the far-field and do not enclose the receivers, the retrieved virtual shot record contains an artifact related to critically refracted waves.

Following equation 1, we crosscorrelate every receiver record in the array with the record at  $\mathbf{x}_B = \mathbf{x}_1$ , the receiver collocated at  $\mathbf{s}_1$ . Figure 2a and 2b shows the real and virtual shot records for this model, respectively. The  $x$ -axes represent the distance between the real or virtual source at  $\mathbf{s}_1 = \mathbf{x}_1$  and a given receiver at  $\mathbf{x}_A$ . In Figure 2b we retrieve the direct-wave arrival from the crosscorrelation between the direct waves, and the refraction artifact, denoted as the *virtual refraction*. The arrival time of the virtual refraction is  $T_c = dr/V_2$ , where  $dr$  is the difference in travel path that critically refracted energy travels between the two receivers (Figure 1). The virtual refraction is produced because of an incomplete source distribution and the far-field radiation approximation inherent within equation 1 (Mikesell et al., 2009). The most intuitive reason for the virtual refraction is that crosscorrelations of reflections from sources past the critical offset from  $\mathbf{x}_1$  (Figure 1) sum constructively during seismic interferometry. This energy is constant across the source array (e.g.,  $T_c$  in Figure 3), and therefore, does not sum destructively when summing the crosscorrelations over all sources.

Comparing Figure 2a and 2b, the virtual source recovers little of the reflected wave. This is because the stationary-phase crosscorrelations (Snieder, 2004) (i.e., energy that sums constructively for the reflected event) occur near the virtual source at  $\mathbf{x}_1$ . In this numerical example, we apply a cosine taper to 25% of sources on each side of the source array in the crosscorrelation gather before creating the virtual shot record (i.e.,  $\mathbf{s}_1$  to  $\mathbf{s}_{55}$  and  $\mathbf{s}_{166}$  to  $\mathbf{s}_{221}$ ). The taper

Manuscript received by the Editor 22 February 2011; revised manuscript received 29 March 2011; published online 7 November 2011.  
<sup>1</sup>Boise State University, Department of Geosciences, Physical Acoustics Laboratory, Boise, Idaho, USA, E-mail: dmikesell@cgiss.boisestate.edu; kaspervanwijk@boisestate.edu.  
© 2011 Society of Exploration Geophysicists. All rights reserved.

suppresses truncation artifacts produced from the incomplete source aperture (Snieder et al., 2006).

In conventional refraction analysis we estimate  $V_1$  and  $V_2$  from the slope of the direct and refracted waves, respectively. We would usually estimate the depth to the interface to be (equation 3-41a in Yilmaz, 2001):

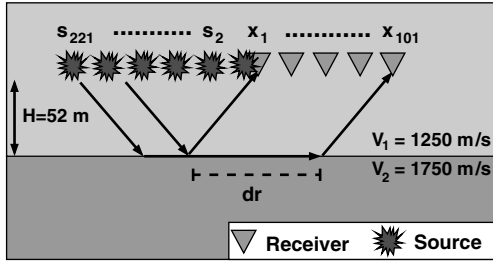


Figure 1. Two-layer acoustic model with  $V_1 = 1250$  m/s,  $V_2 = 1750$  m/s, and  $H = 52$  m. The source increment is 2.5 m and receiver increment is 4 m.

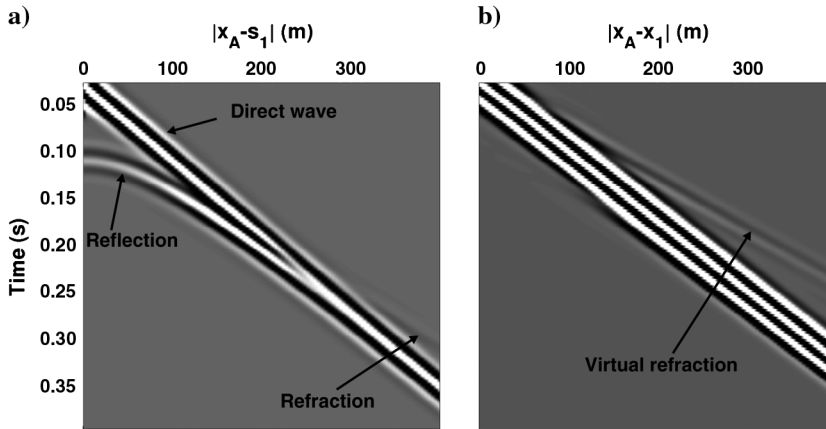


Figure 2. (a) Real shot record and (b) virtual shot record for real and virtual sources at  $s_1 = x_1$ . The virtual shot record contains the direct arrival and the virtual refraction artifact indicated by the arrow.

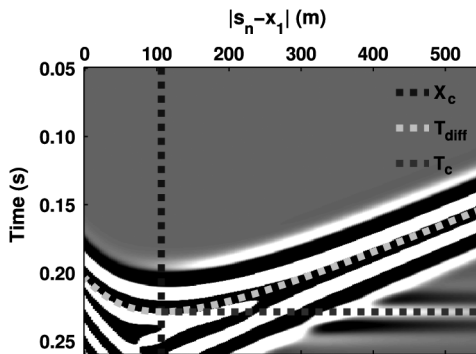


Figure 3. Crosscorrelation gather for  $|x_{101} - x_1| = 400$  m. The critical offset  $X_c$  occurs at the maximum of  $T_{diff}$ .  $T_c$  is the crosscorrelation between the refractions at both receivers and is equal to  $|x_{101} - x_1|/V_2$  in this model.

$$H = \frac{V_1 V_2 t_i}{2\sqrt{V_2^2 - V_1^2}}, \quad (2)$$

where  $t_i$  is the projected refraction intercept time at zero offset. The virtual refraction, on the other hand, has an intercept time  $t_i = 0$  s. Nichols et al. (2010) extract  $H$  and  $V_1$  by estimating  $V_2$  from the moveout of the virtual refraction and picking the critical offset ( $X_c$ ) in the crosscorrelation gather. However, estimating  $X_c$  manually can prove difficult in noisy field data. In the next section, we present an alternative and robust method to estimate  $V_1$  and  $H$  by maximizing the semblance of the energy in the crosscorrelation gather related to this virtual refraction. Finally, we apply this method to estimate the corresponding subsurface properties at the Boise Hydrogeophysical Research Site; a site where standard refraction methods are difficult because ground-roll masks the direct wave and the shallow water-table reflection.

## VELOCITY AND DEPTH ESTIMATION IN THE CROSSCORRELATION DOMAIN

We propose a semblance analysis of the crosscorrelation gather to estimate  $V_1$  and  $H$ , similar to King et al. (2011) and Poliannikov and Willis (2011), but focused on the virtual refraction. Figure 3 shows the crosscorrelation gather for  $|x_{101} - x_1| = 400$  m for all sources in Figure 1. The crosscorrelation between the reflection at  $x_B$  and the refraction at  $x_A$  yields  $T_{diff}$ . We annotate the curve  $T_{diff}$  in Figure 3 as well as indicate  $X_c$  and  $T_c$  — the crosscorrelation between the refractions at both receivers.

For a linear source array, Mikesell et al. (2009) show that the maximum of  $T_{diff}$  occurs at the critical offset  $X_c$  from receiver  $x_B$ . The traveltime difference curve  $T_{diff}$  from a source at  $s_n$  is

$$T_{diff}(\mathbf{x}_A, \mathbf{x}_B) = T_{refr}(\mathbf{x}_A, s_n) - T_{refl}(\mathbf{x}_B, s_n), \quad (3)$$

where the reflection arrival time is

$$T_{refl}(\mathbf{x}_B, s_n) = \sqrt{\left(\frac{|\mathbf{x}_B - s_n|}{V_1}\right)^2 + \left(\frac{2H}{V_1}\right)^2}, \quad (4)$$

and the refraction arrival time is

$$T_{refr}(\mathbf{x}_A, s_n) = \frac{2H \cos \theta_c}{V_1} + \frac{|\mathbf{x}_A - s_n|}{V_2} \quad (5)$$

(derived from equation 10, section 3.2 in Stein and Wysession, 2003). The parameters in equations 4 and 5 are defined in Figure 1, and Snell's Law relates the model velocities to the critical angle,  $\sin(\theta_c) = \frac{V_1}{V_2}$ . With  $|\mathbf{x}_A - s_n| = |\mathbf{x}_B - s_n| + |\mathbf{x}_A - \mathbf{x}_B|$ , equation 3 becomes

$$T_{diff}(\mathbf{x}_A, \mathbf{x}_B) = T_{refr}(\mathbf{x}_B, s_n) - T_{refl}(\mathbf{x}_B, s_n) + \frac{|\mathbf{x}_A - \mathbf{x}_B|}{V_2}. \quad (6)$$

We propose to calculate the  $T_{diff}$  curve for combinations of  $V_1$  and  $H$  for all  $|\mathbf{x}_B - s_n|$ , taking  $V_2$  from the slope of the virtual refraction.

We define the semblance as

$$S_{ij} = \frac{E_{ij}^{\text{out}}}{N \times E_{ij}^{\text{in}}}, \quad (7)$$

where  $N$  is the number of sources in the crosscorrelation gather and  $i$  and  $j$  represent a given  $V_1$  and  $H$ , respectively. The numerator and denominator are the output ( $E^{\text{out}}$ ) and input ( $E^{\text{in}}$ ) energies (Neidell and Taner, 1971) around the arrival of  $T_{\text{diff}}$ :

$$E_{ij}^{\text{out}} = \sum_{n=1}^N \left( \sum_{t=T_{\text{diff}}(i,j,n)-t_w/2}^{T_{\text{diff}}(i,j,n)+t_w/2} C(\mathbf{x}_A, \mathbf{x}_B, \mathbf{s}_n, t) \right)^2 \quad (8)$$

and

$$E_{ij}^{\text{in}} = \sum_{n=1}^N \left( \sum_{t=T_{\text{diff}}(i,j,n)-t_w/2}^{T_{\text{diff}}(i,j,n)+t_w/2} C^2(\mathbf{x}_A, \mathbf{x}_B, \mathbf{s}_n, t) \right), \quad (9)$$

where  $C$  is the crosscorrelated wavefield at  $\mathbf{x}_A$  and  $\mathbf{x}_B$  for source  $\mathbf{s}_n$ , and  $t_w$  is a user-defined time window. Noting that a larger time window will increase stability at the cost of resolution (Poliannikov and Willis, 2011) we use  $t_w = 10$  ms in the following examples and compute  $S_{ij}$  over a range of  $V_1$  and  $H$  values.

### Numerical data example

Figure 4 shows crosscorrelation gathers for different receivers at  $\mathbf{x}_A$  crosscorrelated with the virtual source receiver at  $\mathbf{x}_1$ . The crosscorrelation gathers in Figure 4 are not tapered. From Figure 4a to Figure 4c the distance  $|\mathbf{x}_A - \mathbf{x}_1|$  increases. At smaller  $|\mathbf{x}_A - \mathbf{x}_1|$ , the crosscorrelations of other wave modes overlap  $T_{\text{diff}}$ . However, as  $|\mathbf{x}_A - \mathbf{x}_1|$  increases,  $T_{\text{diff}}$  separates from the other events. Note that Figure 4c is the same as Figure 3; however, we do not see  $T_c$  in Figure 4c because the crosscorrelation of direct waves saturates the gray scale. Figure 5 shows the semblance for the crosscorrelation gathers in Figure 4. It is apparent from Figure 5 that  $T_{\text{diff}}$  must be isolated in time and space in order for the semblance to accurately estimate  $H$  and  $V_1$ . The correct velocity and depth values in this model, as indicated by the star, are  $V_1 = 1250$  m/s and  $H = 52$  m.

### Stacking semblance panels

The maximum semblance offers an estimate of the velocity and depth of the top layer between  $X_c$  and  $\mathbf{x}_1$ . In our laterally homogeneous model, the semblance estimate is independent of  $\mathbf{x}_A$ . Thus, we can stack semblance panels from many  $|\mathbf{x}_A - \mathbf{x}_1|$  to increase the signal-to-noise ratio (S/N). Figure 6a shows the crosscorrelation gather for  $|\mathbf{x}_{101} - \mathbf{x}_1| = 400$  m. We add random zero-mean Gaussian noise to the shot gathers before crosscorrelation. Figure 6a shows that only crosscorrelations related to the large amplitude direct-wave are coherent, and the  $T_{\text{diff}}$  energy is not. The semblance of this crosscorrelation gather (Figure 6b) is equally hard to interpret. However, Figure 6c is the semblance after stacking 20 individual semblance panels from  $|\mathbf{x}_{81} - \mathbf{x}_1| = 320$  m to  $|\mathbf{x}_{101} - \mathbf{x}_1| = 400$  m. The maximum semblance in the stacked panel occurs at  $V_1 = 1250$  m/s and  $H = 58$  m. The maximum semblance estimates the true value of  $V_1$  while estimating  $H$  to within 11.5%.

## FIELD DATA EXAMPLE

The Boise Hydrogeophysical Research Site (BHRS) is a research well-field near Boise, Idaho (USA), developed to study the properties of heterogeneous aquifers using hydrogeological and geophysical tools (Barrash et al., 1999). Figure 7 is a model of the top 4 m at the BHRS showing vertical hammer source and vertical component geophone locations, spaced at a 1-m interval. Based on electronic tape measurements in well X3, approximately 10 m from the receiver array, Johnson (2011) estimates the water-table depth during data collection in 2009 to be approximately 1.7 m below the ground surface. The saturated sand below the water-table has

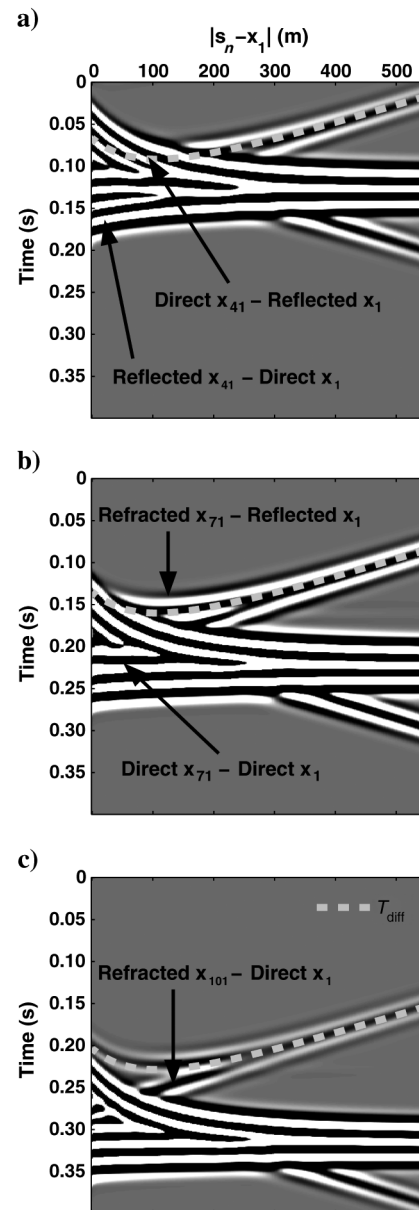


Figure 4. Crosscorrelation gathers for (a)  $|\mathbf{x}_{41} - \mathbf{x}_1| = 160$  m, (b)  $|\mathbf{x}_{71} - \mathbf{x}_1| = 280$  m, and (c)  $|\mathbf{x}_{101} - \mathbf{x}_1| = 400$  m. As  $|\mathbf{x}_A - \mathbf{x}_1|$  increases,  $T_{\text{diff}}$  becomes isolated in time and space.

a larger P-wave velocity than the unsaturated sand above (Moret et al., 2004). Nichols et al. (2010) extracts  $H$  and  $V_1$  by picking the critical offset  $X_c$  in the crosscorrelation gather and estimating  $V_2$  from the moveout of the virtual refraction. This proved to be difficult and conducive to error by the interpreter. In the following, we compare our semblance approach to the approach of Nichols et al. (2010) using their 2009 seismic data.

Figure 8a shows the trace-normalized shot record for source  $s_1$  and offers insight into why our semblance approach might be better suited than conventional refraction methods for characterizing the water table. This shot record is dominated by dispersive

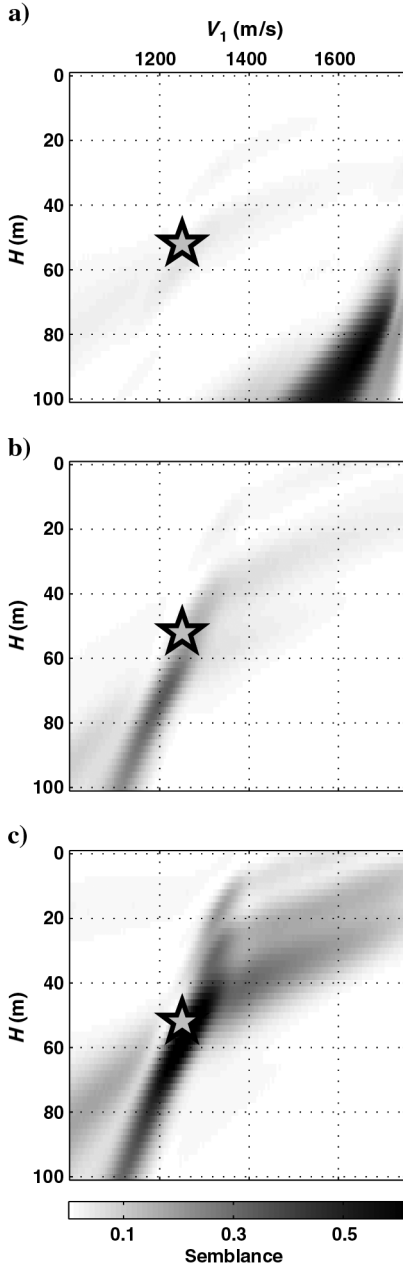


Figure 5. Semblance panels for (a)  $|\mathbf{x}_{41} - \mathbf{x}_1| = 160$  m, (b)  $|\mathbf{x}_{71} - \mathbf{x}_1| = 280$  m, and (c)  $|\mathbf{x}_{101} - \mathbf{x}_1| = 400$  m. The star indicates the correct model parameters.

ground-roll and coherent low-frequency noise from a bridge column located approximately 100 m north of the receiver array. To suppress the ground-roll and bridge noise, we apply a zero-phase trapezoidal filter with corner frequencies 50, 100, 200, and 400 Hz, and a root-mean-square automatic gain control (e.g., p. 85 in Yilmaz, 2001) with a window of 0.05 s (Figure 8b). A coherent refraction from the water table is annotated, but remaining ground-roll and a shallow water table at this site make it difficult to identify a direct or reflected wave. Without the direct wave, we cannot estimate  $V_1$  or  $H$  using the conventional refraction method described in the Introduction.

Nichols et al. (2010) performed SI and used the crosscorrelation gather to manually pick  $X_c$  at the maximum of  $T_{diff}$ . We apply SI to the shot records after applying the processing shown in Figure 8b. Figure 8c is the virtual shot record created using the same tapering procedure as in the numerical data example. The virtual refraction is the dominant arrival that crosses the origin at zero offset. The virtual refraction has the same linear moveout as the real refraction in Figure 8b. To estimate  $V_2$  we take the approach of King and Curtis (2011) and pick the maximum slowness ( $p$ ) at  $\tau = 0$  s after transforming the virtual shot record to the  $\tau$ - $p$  domain (e.g., p. 923 in Yilmaz, 2001). The maximum  $p$  at  $\tau = 0$  gives a virtual refraction velocity of 2778 m/s. The dashed line in Figure 8c defines this moveout velocity in the shot domain. This estimate of  $V_2$  agrees well with the saturated velocity estimate of 2700 m/s from Nichols et al. (2010) and Moret et al. (2004).

From here, our approach differs from Nichols et al. (2010) in how we estimate the top layer depth and velocity. We perform a semblance analysis on the crosscorrelation gather, first normalizing each trace in the crosscorrelation gather. We stack 30 semblance panels over the largest offsets ranging from  $|\mathbf{x}_{29} - \mathbf{x}_1| = 28$  m to  $|\mathbf{x}_{59} - \mathbf{x}_1| = 58$  m and estimate  $V_1$  and  $H$  from the maximum semblance. Figure 9 shows the summed semblance panel with maximum semblance at 1.9 m and 395 m/s (white star). The black star denotes the estimate from Nichols et al. (2010) and the dashed line indicates the water-table depth from Johnson (2011). Taking  $V_1 = 400$  m/s from Moret et al. (2004) and  $H = 1.7$  m from direct measurements by Johnson (2011), we estimate  $V_1$  within  $|395 - 400|/400 \approx 1\%$  and  $H$  within  $|1.9 - 1.7|/1.7 \approx 11\%$ .

## DISCUSSION

In both the numerical and field data examples, it appears that our estimates of  $V_1$  and  $H$  are correlated. This can be seen in the equations 3, 4, 5, 6, where the term  $2H/V_1$  appears repeatedly. The term  $V_1$  appears independent from  $H$  once in these equations, which may be the reason for a better resolved  $V_1$  estimate. To estimate the unsaturated layer depth and velocity, Nichols et al. (2010) pick the critical offset in the crosscorrelation gather, and the critical time in the real shot record. They estimate the critical offset  $X_c$  at 1.3 m in this area of the BHRS. This requires a dense source spacing in order to sample the stationary-phase point in the crosscorrelation gather, and dense receiver spacing (0.25 m) to identify the reflection. Therefore, Nichols et al. (2010) use a 0.1 m source spacing for the 2 m closest to the receiver array, and then change to 1 m for sources past 2 m. Using the values from the maximum semblance, we estimate

$$X_c = \frac{2V_1H}{\sqrt{V_2^2 - V_1^2}} = 0.55 \text{ m.} \quad (10)$$

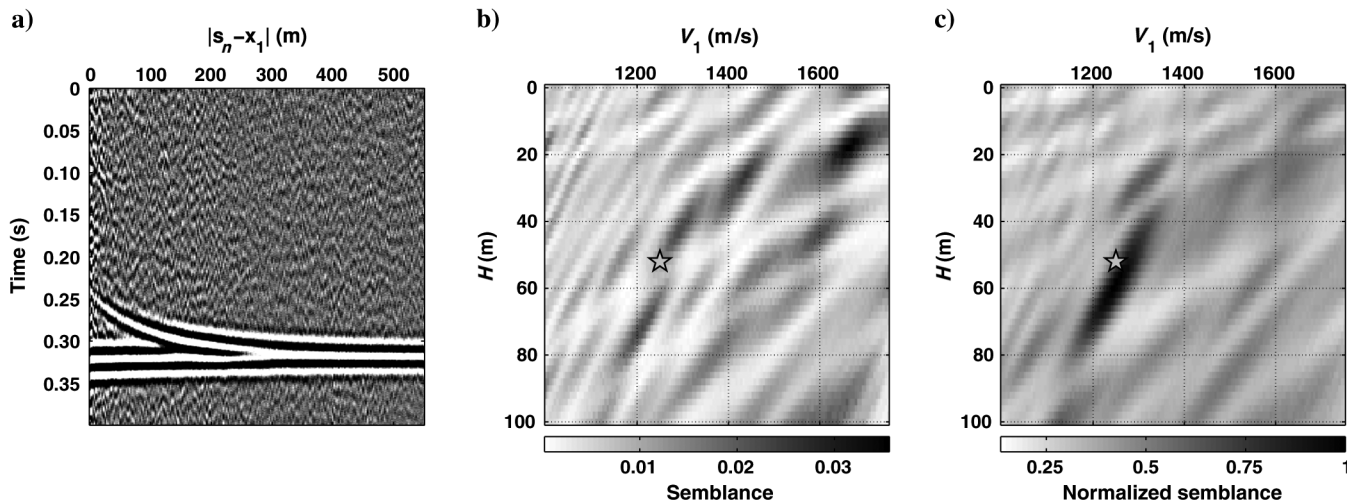


Figure 6. Crosscorrelation gather for (a)  $|x_{101} - x_1| = 400$  m. We add random zero-mean Gaussian noise before crosscorrelation so that  $T_{diff}$  is no longer visible. (b) Semblance panel for the crosscorrelation gather. (c) Semblance panel after stacking 20 semblance panels from  $|x_{81} - x_1| = 320$  m to  $|x_{101} - x_1| = 400$  m.

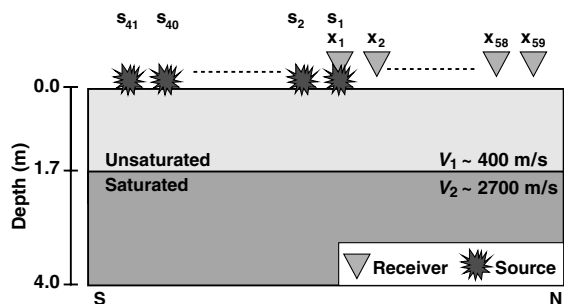


Figure 7. Boise Hydrogeophysical Research Site seismic model. Source and receiver spacing is 1 m.

In either case, the critical offset is on the order of the 1-m spacing we used in the semblance method, but our method does not require that we finely sample so as not to miss  $X_c$ . There is also no need to manually pick the stationary-phase point, which avoids interpreter error. Considering Figure 8b, we feel it is difficult to identify the reflected wave, and thus, the critical time needed in the method presented by Nichols et al. (2010).

Finally, we are able to increase the S/N by stacking multiple semblance panels. The laterally homogeneous numerical data example shows that stacking multiple semblance panels improves estimates of  $V_1$  and  $H$ . In the case of lateral heterogeneity, stacking semblance panels is valid as long as lateral heterogeneity is on the order of the distance between the receivers used in the crosscorrelation gathers. Overall, the semblance approach has advantages to current refraction characterization methods. For example, there is no first break picking, only an estimate of the virtual refraction velocity at  $\tau = 0$  s

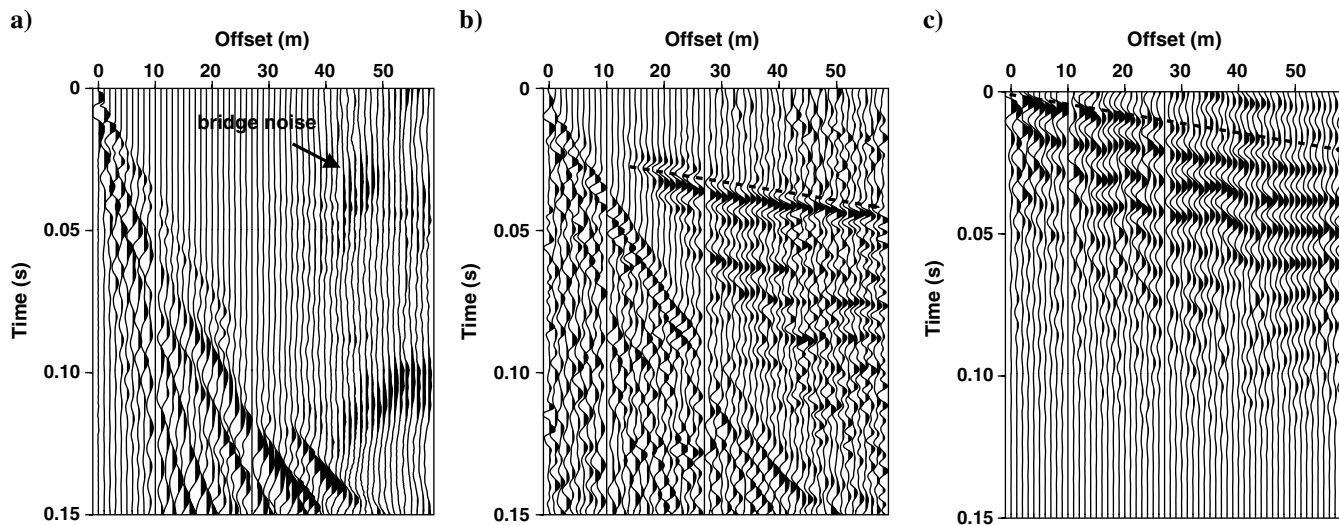


Figure 8. (a) Trace-normalized shot record from a sledgehammer source at the first receiver location. (b) AGC and band-pass filtered shot record—dash indicates water-table refraction. (c) Trace-normalized virtual shot record—dash indicates virtual refraction.

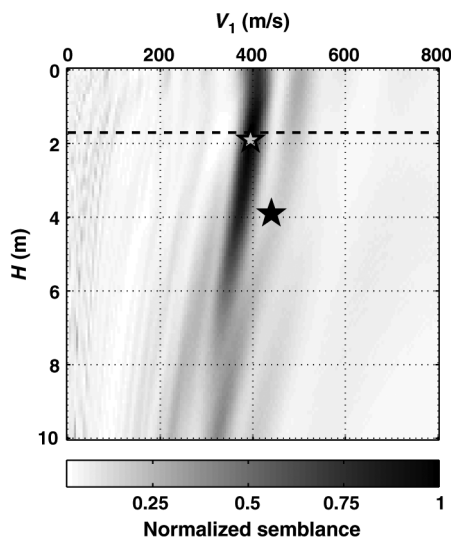


Figure 9. Sum of 30 semblance panels over the range of  $|\mathbf{x}_{29} - \mathbf{x}_1| = 28$  m to  $|\mathbf{x}_{59} - \mathbf{x}_1| = 58$  m. The white star denotes the maximum semblance, which occurs at 1.9 m and 395 m/s. The black star denotes the estimate from Nichols et al. (2010), and the dashed line indicates the water-table depth from Johnson (2011).

in the  $\tau$ - $p$  domain at each virtual shot location, and a semblance maximum for  $H$  and  $V_1$ .

We do not explicitly show how this method extends to multiple layers, but King et al. (2011) present a boot-strapping method whereby they estimate the interval velocity and thickness of multiple horizontal layers using a semblance method with a  $T_{\text{diff}}$  related to primary and multiple reflections. King and Curtis (2011) also use refraction artifacts in a marine setting to estimate the interval velocity of multiple layers by looking at repeating brightspots in a  $\tau$ - $p$  transformed virtual shot record. Finally, our analysis is not restricted to horizontal layers. Poliannikov and Willis (2011) show a crosscorrelation gather semblance method for dipping layers using reflections from those layers; we could parametrize  $T_{\text{diff}}$  to incorporate a dip parameter. This would require solving a three-parameter semblance.

## CONCLUSIONS

Virtual refractions in field applications of seismic interferometry are often present because acquisition requirements for exact recovery of the Green's function between receivers are not met. For a horizontal two-layer model, we estimate the velocity of the faster layer from the slope of the virtual refraction. Using a semblance analysis, we find the velocity and depth of the slower layer. Stacking multiple semblance panels at a single virtual shot location increases the signal-to-noise ratio and gives an improved estimate of these parameters. This approach offers a robust alternative to classical refraction methods.

## ACKNOWLEDGMENTS

We are grateful to Alison Malcolm and Maria Gabriela Melo Silva for discussions on crosscorrelation-domain processing, and to Josh Nichols and Emily Park for the BHRS seismic data collection. We thank the developers of SPECSEM2D seismic modeling code and Seismic Unix processing code. This manuscript was greatly improved by comments from Kees Wapenaar and Simon King. The BHRS has been funded by the US Army Research Office grant DAAH04-96-1-0318 and US EPA grants X-970085-01-0, X-96004601-0, and X-96004601-1.

## REFERENCES

- Bakulin, A., and R. Calvert, 2006, The virtual source method: Theory and case study: *Geophysics*, **71**, no. 4, S1139–S1150, doi: [10.1190/1.2216190](https://doi.org/10.1190/1.2216190).
- Barrash, W., T. Clemo, and M. D. Knoll, 1999, Boise hydrogeophysical research site (BHRS): Objectives, design, initial geostatistical results: Proceedings of SAGEEP99, the Symposium on the Application of Geophysics to Engineering and Environmental Problems, 389–398.
- Johnson, B., 2011, Characterization of evapotranspiration in the riparian zone of the Lower Boise River, with implications for groundwater flow: Master's thesis, Boise State University.
- King, S., and A. Curtis, 2011, Velocity analysis using reflections and refractions in seismic interferometry: *Geophysics*, this issue.
- King, S., A. Curtis, and T. L. Poole, 2011, Interferometric velocity analysis using physical and nonphysical energy: *Geophysics*, **76**, no. 1, SA35–SA49, doi: [10.1190/1.3521291](https://doi.org/10.1190/1.3521291).
- Komatitsch, D., and J. Tromp, 2002, Spectral-element simulations of global seismic wave propagation—I. Validation: *Geophysical Journal International*, **149**, 390–412, doi: [10.1046/j.1365-246X.2002.01653.x](https://doi.org/10.1046/j.1365-246X.2002.01653.x).
- Komatitsch, D., and J.-P. Vilotte, 1998, The spectral element method: An efficient tool to simulate the seismic response of 2D and 3D geological structures: *Bulletin of the Seismological Society of America*, **88**, 368–392.
- Mehta, K., R. Snieder, R. Calvert, and J. Sheiman, 2008, Acquisition geometry requirements for generating virtual-source data: *The Leading Edge*, **27**, 620–629, doi: [10.1190/1.2919580](https://doi.org/10.1190/1.2919580).
- Mikesell, D., K. van Wijk, A. Calvert, and M. Haney, 2009, The virtual refraction: Useful spurious energy in seismic interferometry: *Geophysics*, **74**, no. 3, A13–A17, doi: [10.1190/1.3095659](https://doi.org/10.1190/1.3095659).
- Moret, G. J., W. P. Clement, M. D. Knoll, and W. Barrash, 2004, VSP traveltimes inversion: Near-surface issues: *Geophysics*, **69**, 345–351, doi: [10.1190/1.1707053](https://doi.org/10.1190/1.1707053).
- Neidell, N. S., and M. T. Taner, 1971, Semblance and other coherency measures for multichannel data: *Geophysics*, **36**, 482–497, doi: [10.1190/1.1440186](https://doi.org/10.1190/1.1440186).
- Nichols, J., T. D. Mikesell, and K. van Wijk, 2010, Application of the virtual refraction to near-surface characterization at the Boise Hydrogeophysical Research Site: *Geophysical Prospecting*, **58**, 1011–1022.
- Poliannikov, O. V., and M. E. Willis, 2011, Interferometric correlogram-space analysis: *Geophysics*, **76**, no. 1, SA9–SA17, doi: [10.1190/1.3519875](https://doi.org/10.1190/1.3519875).
- Snieder, R., 2004, Extracting the Green's function from the correlation of coda waves: A derivation based on stationary phase: *Physical Review E*, **69**, 046610, doi: [10.1103/PhysRevE.69.046610](https://doi.org/10.1103/PhysRevE.69.046610).
- Snieder, R., K. Wapenaar, and K. Larner, 2006, Spurious multiples in seismic interferometry of primaries: *Geophysics*, **71**, no. 4, S1111–S1124, doi: [10.1190/1.2211507](https://doi.org/10.1190/1.2211507).
- Stein, S., and M. Wysession, 2003, An introduction to seismology, earthquakes and earth structure: Wiley-Blackwell.
- Wapenaar, K., and J. Fokkema, 2006, Green's function representations for seismic interferometry: *Geophysics*, **71**, no. 4, S133–S146, doi: [10.1190/1.2213955](https://doi.org/10.1190/1.2213955).
- Wapenaar, K., J. Thorbecke, and D. Draganov, 2004, Relations between reflection and transmission responses of three-dimensional inhomogeneous media: *Geophysical Journal International*, **156**, no. 2, 179–194, doi: [10.1111/gji.2004.156](https://doi.org/10.1111/gji.2004.156).
- Yilmaz, O., 2001, Seismic data analysis: SEG.